Pergamon

*Int. J. Solids Structures* Vol. 31, No. 3, pp. 391–415, 1994

0020–7683/94 $6.00 + .00

# TOPOLOGICAL MEASURE OF BRITTLE FRAGMENTATION

Z. YONG and M. T. HANSON
Department of Engineering Mechanics

and

R. KOVACEVIC
Department of Mechanical Engineering, University of Kentucky, Lexington, KY 40506-0046, U.S.A.

(*Received* 20 *October* 1992; *in revised form* 6 *July* 1993)

**Abstract**—A new approach for quantitative analysis of fragmentation for brittle materials is developed with the aid of axioms of continuum mechanics, fracture mechanics and topology. The principles of energy balance are used to establish the field equations for the surface and volume of a fragment which is homeomorphic to a sphere. The global and local geometric constraints on fragmentation are unveiled as a deterministic description of a crack network by use of the Euler theorem and energy transformation. Several physical phenomena are revealed in the present research. A new physical parameter, the dissipative rate of surface energy, is derived which provides a theoretical basis for understanding the latest experimental results. One of the applications of the model is to understand some basic parameters for formation of a branching crack network with a single source. Theoretical analysis is in very good agreement with experimental results.

## 1. INTRODUCTION

The comprehensive description and quantitative estimation of fragmentation for brittle materials caused by dynamic loading is a challenging topic researchers have faced in the mechanics field for some time. Presently, the fragmentation process is no longer limited to large scale destructive purposes as in mining, civil and defense engineering. It can also be seen in manufacturing during the cutting process of brittle materials by abrasive jet [e.g. Gulden (1979)]. Also research on the collisional fragmentation damage of satellites caused by debris is emphasized by McKnight (1991). These examples suggest the increasing need for accurate quantitative analysis of fragmentation. Furthermore, from the standpoint of crack network formation, a similar fragmentation process in solid materials is also observed on the micro-level during material failure and deformation (Meakin, 1991). To some degree, examination of crack network formation may provide insight into the intrinsic relationship between the mechanism of microcrack formation and the macro-failure of materials.

From the point of view of continuum mechanics, any attempt to make a quantitative analysis of fragmentation parameters, such as energy consumption or fragment sizes and their distribution, will encounter several difficulties. First, the instantaneous alteration of a continuum medium to a large number of fragments with possibly different physical states brings about great difficulties in the establishment of a problem formulation. Secondly, the wide diversity of size and shape of fragments provides a complicated pattern for classical geometric analysis. Thus to a certain degree [as described by Grady (1990)] it is true that the whole process of fragmentation might be a black box problem because so far very few physical and geometric constraints have been found on the process. More specifically, fragmentation my be ascribed as the consequence of the branching, diverging and interacting of cracks. However, development of dynamic fracture mechanics, a vital stage related to understanding mechanisms of fragmentation, is still in the initial stage because of formidable difficulties in theoretical approaches. In fact, many significant investigations have depended heavily on experimental analysis. For instance, Arakawa and Takahashi (1991a, b) recently discovered an important criterion for crack branching in their experimental investigation,

but its physical meaning seems to be unknown. Therefore an essential task for the quantitative investigation of fragmentation is to find both the physical and geometric invariants behind this complicated process.

If the direction of research work on fragmentation is shifted from a traditional point of view to a new one, there is good cause for optimism. First of all, the axioms of mass, momentum and thermodynamics always hold however complex a fragmenting process is. In addition, geometrically speaking, the division of a closed surface is not arbitrary but is deterministic in a topological sense due to constraints imposed by the Euler theorem (Blackett, 1967). Furthermore, careful observation of a large number of fragments of various materials indicates that despite big differences in size and shape, the closed surface of a fragment can be defined to be homeomorphic to a sphere. The fragmentation of a solid body may be considered as the loss of continuity of a point set in a global sense but local continuity holds for any subset described by a single fragment.

The application of energy balance may be one of the most important approaches to a quantitative description of fragmentation which has been used for a long time by many researchers. The equation for the estimation of fragment size with spherical symmetry by Grady (1982) may be one of the successful results. It can be verified from general principles that under certain conditions the Grady model is a rational model and has potential to become a model for non-spherical problems. Many incisive analyses and an extensive review on the subject can be found in the published reports given by Grady (1982, 1988, 1990), Grady and Kipp (1985) and Kipp and Grady (1985). Recently, a general theoretical analysis on the fragmentation of composite materials has been conducted by Kobelev (1990) in which three-dimensional cases are discussed. However, the basic concept of Kobelev's investigation, transformation of kinetic energy into surface energy, is in disagreement with the well known theory [strain energy transformed into surface energy (Griffith, 1920)].

A careful review of the previous models reveals that it is very difficult to obtain a unified physical understanding from them. Therefore it is natural for the present research to first focus on understanding the physical basis of fragmentation by employing the axioms of continuum mechanics. After a new physical parameter for the dynamic process is determined through theoretical analysis, a field equation is established which is rooted in transformation of strain energy into surface energy during crack extension. In the geometric analysis, attention is turned to discussion of geometric constraints, including global and local constraints on fragmentation controlled by Euler's theorem and energy consumption. An example analysed subsequently is focused on the treatment of a single element of a symmetric branching crack network with one origin.

## 2. PHYSICAL BACKGROUND

In the subsequent discussion, mathematically speaking, a fragment is referred to as a topological point set $\aleph$ of three-dimensional space. A map transforming $\aleph$ to another set is required to be one-to-one and onto. The physical meaning of this definition is that a fragment can not be broken. In other words, a fragment is specified as a geometrically stable structure during fragmentation. As shown in Fig. 1, formation of a fragment is divided into four states. State I stands for the initial state of no deformation for any geometric element, the subset of $\aleph$. The position of a point $X$ in the state is denoted by the vector $\mathbf{X}$ under material coordinates corresponding to the reference configuration $\kappa$, $\mathbf{X} = \kappa(X)$. State II is just prior to the occurrence of cracks along the boundary $\partial\aleph$ of $\aleph$. State II is sometimes called the critical state. The appearance and growth of cracks along $\partial\aleph$ is defined as state III. It is important to note that state III actually covers a process instead of a specific moment. The moment at which a complete fragment forms is defined to be state IV. This might not occur for a non-closed crack contour. In this case, state IV represents the arrest of cracks and hence a fragment is not a free body. The position of any point in states II–IV is described under spatial coordinates by the vector $\mathbf{x}$:

$$\mathbf{x} = \chi(X, t) = \chi_\kappa(\mathbf{X}, t), \tag{1}$$

called the deformation function relative to the reference configuration. All discussions

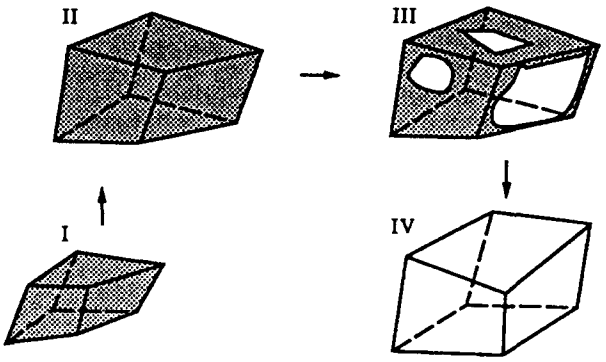


Fig. 1. The four steps of forming a fragment.

throughout the paper are founded on the above division. For a fragmentation event, the four states do not happen simultaneously for each fragment, this is one of the complex characteristics of fragment formation.

To understand the conversion of energy from one form to another during fragmentation, it is very important to decouple, if possible, the energy from its previous form. When the axioms of balance of mass and angular momentum hold for all the points of $\aleph$, the local statements of the axioms for the balance of linear momentum and energy are written as (Leigh, 1968; Bowen, 1989)

$$\rho\ddot{\mathbf{x}} = \operatorname{div}\mathbf{T} + \rho\mathbf{b} \tag{2}$$

and

$$\rho(\dot{\varepsilon} + \tfrac{1}{2}\dot{\dot{\mathbf{x}}}^2) = \operatorname{div}(\mathbf{T}\dot{\mathbf{x}}) - \operatorname{div}\mathbf{q} + \rho\dot{\mathbf{x}}\cdot\mathbf{b} + \rho r. \tag{3}$$

respectively. In (2) and (3), $\rho$ is the density of the medium, $\mathbf{b}$ the body force density, $\mathbf{T}$ the stress tensor, $\varepsilon$ the internal energy density, $\mathbf{q}$ the heat flux vector per unit area and $r$ is the heat supply density. The meaning of density above (except for $\rho$) is referred to as per unit mass. Here "div" stands for the divergence of a function with respect to the spatial coordinate $\mathbf{x}$ and "$\cdot$" on the top of a function denotes the derivative of a function with respect to time $t$. Scalar multiplication of eqn (2) by $\dot{\mathbf{x}}$ produces

$$\rho\dot{\mathbf{x}}\cdot\ddot{\mathbf{x}} = \tfrac{1}{2}\rho\dot{\dot{\mathbf{x}}}^2 = \dot{\mathbf{x}}\cdot\operatorname{div}\mathbf{T} + \rho\dot{\mathbf{x}}\cdot\mathbf{b}. \tag{4}$$

Subtracting (4) from (3) leads to

$$\rho\dot{\varepsilon} = \operatorname{div}(\mathbf{T}\dot{\mathbf{x}}) - \dot{\mathbf{x}}\cdot\operatorname{div}\mathbf{T} - \operatorname{div}\mathbf{q} + \rho r. \tag{5}$$

Since

$$\operatorname{div}(\mathbf{T}\dot{\mathbf{x}}) = \operatorname{tr}(\mathbf{TL}) + \dot{\mathbf{x}}\cdot\operatorname{div}\mathbf{T} \tag{6}$$

and

$$\operatorname{tr}(\mathbf{TL}) = \operatorname{tr}[\mathbf{T}(\mathbf{D}+\mathbf{W})] = \operatorname{tr}(\mathbf{TD}) + \operatorname{tr}(\mathbf{TW}) = \operatorname{tr}(\mathbf{TD}), \tag{7}$$

eqn (5) becomes

$$\rho\dot{\varepsilon} = \mathrm{tr}\,(\mathbf{TL}) - \mathrm{div}\,\mathbf{q} + \rho r = \mathrm{tr}\,(\mathbf{TD}) - \mathrm{div}\,\mathbf{q} + \rho r, \tag{8}$$

where $\mathbf{L} = \mathrm{grad}\,\dot{\mathbf{x}}(\mathbf{x}, t)$ is the velocity gradient at $(\mathbf{x}, t)$, $\mathbf{D} = (\mathbf{L}+\mathbf{L}^{\mathrm{T}})/2$ the stretching tensor and $\mathbf{W} = (\mathbf{L}-\mathbf{L}^{\mathrm{T}})/2$ the spin tensor. Equation (8) illustrates that the rate of the internal energy can be separated from the total energy due to the decomposition of the work rate $\mathrm{div}\,(\mathbf{T}\dot{\mathbf{x}})$ per unit volume into two parts which alter the kinetic energy and the internal energy. Different forms of energy balance can be obtained by integrating eqns (3), (4) and (8) in the volume region $\chi(\aleph, t)$ from the initial time $t_0$ to the current time $t$. The kinetic energy $E_{\mathrm{k}}$ is of the form

$$E_{\mathrm{k}} = \int_{t_0}^{t} \mathrm{d}t \int_{\chi(\aleph,t)} \tfrac{1}{2}\rho\dot{\mathbf{x}}^{2}\,\mathrm{d}v = \int_{t_0}^{t} \mathrm{d}t \int_{\chi(\aleph,t)} (\dot{\mathbf{x}}\cdot\mathrm{div}\,\mathbf{T} + \rho\dot{\mathbf{x}}\cdot\mathbf{b})\,\mathrm{d}v, \tag{9}$$

and the internal energy $E_{\mathrm{i}}$ is written as

$$E_{\mathrm{i}} = \int_{t_0}^{t} \mathrm{d}t \int_{\chi(\aleph,t)} \rho\dot{\varepsilon}\,\mathrm{d}v = \int_{t_0}^{t} \mathrm{d}t \int_{\chi(\aleph,t)} [\mathrm{tr}\,(\mathbf{TD}) - \mathrm{div}\,\mathbf{q} + \rho r]\,\mathrm{d}v, \tag{10}$$

where the total energy $E_{\mathrm{t}} = E_{\mathrm{k}} + E_{i}$ becomes

$$\begin{aligned} E_{\mathrm{t}} &= \int_{t_0}^{t} \mathrm{d}t \int_{\chi(\aleph,t)} [\mathrm{div}\,(\mathbf{T}\dot{\mathbf{x}}) - \mathrm{div}\mathbf{q} + \rho\dot{\mathbf{x}}\cdot\mathbf{b} + \rho r]\,\mathrm{d}v \\ &= \int_{t_0}^{t} \mathrm{d}t \int_{\partial\chi(\aleph,t)} (\mathbf{T}\dot{\mathbf{x}} - \mathbf{q})\cdot\mathbf{ds} + \int_{t_0}^{t} \mathrm{d}t \int_{\chi(\aleph,t)} (\rho\dot{\mathbf{x}}\cdot\mathbf{b} + \rho r)\,\mathrm{d}v. \end{aligned} \tag{11}$$

Here (9)–(11) are universal identities for any time interval and any spatial region.

In terms of pure kinetic energy and internal energy, the measure of $E_{\mathrm{k}}$ and $E_{\mathrm{i}}$ is meaningful only with respect to the reference configuration which is instantaneously consistent with the current state. This results since $\mathbf{D}$ may not be a pure rate of stretching and $\mathbf{W}$ may not be a pure rate of rotation. This is easily seen by substitution of the polar decomposition of the deformation gradient $\mathbf{F} = \mathrm{GRAD}\chi_{\kappa}(\mathbf{X}, t) = \mathbf{RU}$ into the expressions for $\mathbf{D}$ and $\mathbf{W}$ as

$$\mathbf{D} = \tfrac{1}{2}(\dot{\mathbf{F}}\mathbf{F}^{-1} + \mathbf{F}^{-\mathrm{T}}\dot{\mathbf{F}}^{\mathrm{T}}) = \tfrac{1}{2}\mathbf{R}(\dot{\mathbf{U}}\mathbf{U}^{-1} + \mathbf{U}^{-1}\dot{\mathbf{U}})\mathbf{R}^{\mathrm{T}} \tag{12}$$

and

$$\mathbf{W} = \dot{\mathbf{R}}\mathbf{R}^{\mathrm{T}} + \tfrac{1}{2}\mathbf{R}(\dot{\mathbf{U}}\mathbf{U}^{-1} - \mathbf{U}^{-1}\dot{\mathbf{U}})\mathbf{R}^{\mathrm{T}}, \tag{13}$$

where $\mathbf{R}$ is the rotation tensor and $\mathbf{U}$ is the right stretch tensor.

When a thermodynamic process is assumed to be adiabatic, in particular, to be a purely mechanical process of an elastic material, the internal energy $E_{\mathrm{i}}$ is sometimes called the strain energy since the constitutive equation for the elastic material can be written as

$$\mathbf{T} = \rho\mathbf{F}\frac{\partial u_{\kappa}(\mathbf{F},\mathbf{X})^{\mathrm{T}}}{\partial\mathbf{F}} = \rho\frac{\partial u_{\kappa}(\mathbf{F},\mathbf{X})}{\partial\mathbf{F}}\mathbf{F}^{\mathrm{T}}, \tag{14}$$

because of constraint of the entropy inequality $-\rho\dot{\varepsilon} + \mathrm{tr}\,(\mathbf{TL}) \geqslant 0$ where $\varepsilon = u_{\kappa}(\mathbf{F}, \mathbf{X})$. Note that in this circumstance the entropy remains unchanged.

For convenience in the analysis for small deformation, eqns (10) and (11) are written in the material forms

$$E_i = \int_{t_0}^{t} \mathrm{d}t \int_{\kappa(\aleph)} \rho_R \dot{\varepsilon}\, \mathrm{d}V = \int_{t_0}^{t} \mathrm{d}t \int_{\kappa(\aleph)} [\mathrm{tr}\,(\mathbf{T}_R^T \mathbf{F}) - \mathrm{Div}\mathbf{q}_R + \rho_R r]\, \mathrm{d}V \tag{15}$$

and

$$\begin{aligned} E_t &= \int_{t_0}^{t} \mathrm{d}t \int_{\kappa(\aleph)} [\mathrm{Div}\,(\mathbf{T}_R^T \dot{\mathbf{x}}) - \mathrm{Div}\mathbf{q}_R + \rho_R \dot{\mathbf{x}} \cdot \mathbf{b} + \rho_R r]\, \mathrm{d}V \\ &= \int_{t_0}^{t} \mathrm{d}t \int_{\partial\kappa(\aleph)} (\mathbf{T}_R^T \dot{\mathbf{x}} - \mathbf{q}_R) \cdot \mathrm{d}\mathbf{S} + \int_{t_0}^{t} \mathrm{d}t \int_{\kappa(\aleph)} (\rho_R \dot{\mathbf{x}} \cdot \mathbf{b} + \rho_R r)\, \mathrm{d}V, \end{aligned} \tag{16}$$

where $\mathbf{q}_R = |\det\mathbf{F}|\mathbf{F}^{-1}\mathbf{q}$, $\rho_R = |\det\mathbf{F}|\rho$ and $\mathbf{T}_R = |\det\mathbf{F}|\mathbf{T}\mathbf{F}^{-T}$ which is called the first Piola–Kirchhoff stress tensor.

From (9) and (10), since the kinetic energy and internal energy resulting from the work done by external loadings are not coupled, their conversion to any other energy form can be examined independently. To simplify the present analysis, attention is here focused on an adiabatic process with no dissipation of energy except for surface energy.

One of the major issues for a theoretical analysis of fragmentation is to determine which energy form, internal energy or kinetic energy or both, is the major source converted into surface energy. The answer to this question in the present research work is the internal energy, i.e. strain energy, because:

(a) the fracture between two groups of particles is such an event which causes the loss of recovery capability of those particles separated by a crack;

(b) the internal energy does not necessarily depend on inertial effects. In other words, under static or quasi-static loading conditions, unlike kinetic energy, the internal energy is not equal to zero;

(c) the previous experimental results support the assertion [e.g. Kobayashi *et al.* (1980) and Kanninen and Popelar (1985)].

To understand the physical process of energy transformation during fragmentation, the crack propagation under quasi-static Mode I conditions is analysed in detail in the following.

As shown in Fig. 2, a uniform pressure $\sigma(t)$ is applied on the surfaces of a crack with length $2c$ embedded in an infinite, linear, homogeneous and isotropic medium with unit thickness and no body force. Each half infinite body is considered here as a fragment. As $t = t_{II}$, $\sigma(t)$ reaches the critical value $\sigma(t_{II})$ and the crack begins to grow. From $t_{II}$ to $t_{IV}$, only the fraction of work done by $\sigma(t)$ which is dissipated by the resistance to crack extension is the significant part for analysis of surface energy. Therefore, during $\Delta t = t_{IV} - t_{II}$, $\sigma(t)$ is chosen to be just enough to drive the extension of the crack. At $t = t_{IV}$, the crack grows to the maximum $a(t_{IV}) = a_0$ and arrests while $\sigma(t)$ decreases down to zero at $t = t_V$. The

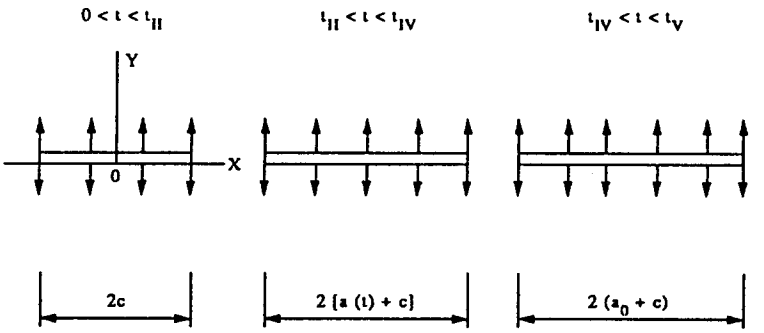


Fig. 2. The initial propagation and arresting states of a straight crack.

maximum value of $\sigma(t)$ is bounded so that the extension of the crack is self-similar, i.e. no branching or curving occurs during extension.

Presently it will be assumed that the crack extension is quasi-static and deformation remains infinitesimal. In this case, the first Piola–Kirchhoff stress tensor becomes a symmetric tensor $\mathbf{T}_R = \mathbf{T}_R^T$. Based on the exact solutions corresponding to static conditions, the displacement and loading of a crack surface are given in the forms

$$\text{I–II:}\quad \begin{aligned} &\sigma(t) = \text{an arbitrary function}, \quad 0 \leqslant t \leqslant t_{II},\\ &\sigma(0) = 0, \quad \sigma(t_{II}) = \frac{K_{dc}}{\sqrt{c}},\\ &v(t,x) = \frac{2\sigma(t)}{E_d}\sqrt{c^2-x^2}, \qquad |x| \leqslant c, \end{aligned} \tag{17}$$

$$\text{II–IV:}\quad \begin{aligned} &\sigma(t) = \frac{K_d(t)}{\sqrt{a(t)+c}}, \quad K_d(t_{II}) = K_{dc}, \quad t_{II} \leqslant t \leqslant t_{IV},\\ &a(t_{II}) = 0, \quad a(t_{IV}) = a_0,\\ &v(t,x) = \frac{2\sigma(t)}{E_d}\sqrt{[a(t)+c]^2-x^2}, \qquad |x| \leqslant a(t)+c, \end{aligned} \tag{18}$$

$$\text{IV–V:}\quad \begin{aligned} &\sigma(t) = \text{an arbitrary function}, \qquad t_{IV} \leqslant t \leqslant t_V,\\ &\sigma(t_{IV}) = \frac{K_{da}}{\sqrt{a_0+c}}, \quad K_d(t_{IV}) = K_{da}, \quad \sigma(t_V) = 0,\\ &v(t,x) = \frac{2\sigma(t)}{E_d}\sqrt{(a_0+c)^2-x^2}, \qquad |x| \leqslant a_0+c, \end{aligned} \tag{19}$$

where $K_{dc}$ is the dynamic fracture toughness, $K_d(t)$ is the dynamic stress intensity factor, $K_{da}$ is the stress intensity factor as the crack arrests and $E_d$ is the dynamic elastic modulus which should be replaced by $(E_d/(1-\nu^2))$ for plane strain problems where $\nu$ is the Poisson ratio. In addition, stress components are equal to zero at infinity and

$$\dot{v}(t,x) = 0, \quad 0 \leqslant t \leqslant t_V, \quad a(t)+c < |x|, \tag{20}$$

because of the symmetric property of the problem. From $t = 0$ to $t_v$, a fraction of the work done by the input loading should be converted into surface energy. The value can be obtained by substitution of (17)–(19) into the right-hand side of (16) and then integrating, leading to

$$\tfrac{1}{2}E_t = \int_0^{t_v} \mathrm{d}t \int_{\partial\kappa(S)} (\mathbf{T}_R\dot{\mathbf{x}})\cdot \mathrm{d}\mathbf{S} = E_1 + E_2 + E_3 = \frac{\pi}{E_d}\int_{t_{II}}^{t_{IV}} K_d^2(t)\dot{a}(t)\,\mathrm{d}t, \tag{21}$$

where $\dot{a}(t)$ is the velocity of crack propagation and

$$E_1 = \frac{2}{E_d}\int_0^{t_{II}} \sigma(t)\dot{\sigma}(t)\,\mathrm{d}t \int_{-c}^{c} \sqrt{c^2-x^2}\,\mathrm{d}x = \frac{\pi K_{dc}^2}{2E_d}c, \tag{22}$$

$$\begin{aligned} E_2 = \frac{2}{E_d}\int_{t_{II}}^{t_{IV}} \sigma(t)\,\mathrm{d}t \int_{-a(t)-c}^{a(t)+c} \left\{\dot{\sigma}(t)\sqrt{[a(t)+c]^2-x^2} + \frac{\sigma(t)[a(t)+c]\dot{a}(t)}{\sqrt{[a(t)+c]^2-x^2}}\right\}\mathrm{d}x\\ = \frac{\pi}{2E_d}[K_{da}^2(a_0+c) - K_{dc}^2 c] + \frac{\pi}{E_d}\int_{t_{II}}^{t_{IV}} K_d^2(t)\dot{a}(t)\,\mathrm{d}t, \end{aligned} \tag{23}$$

$$E_3 = \frac{2}{E_d}\int_{t_{IV}}^{t_V} \sigma(t)\dot{\sigma}(t)\,dt \int_{-a_0-c}^{a_0+c} \sqrt{(a_0+c)^2-x^2}\,dx = -\frac{\pi K_{da}^2}{2E_d}(a_0+c). \tag{24}$$

Note that the equation

$$\int_{-\infty}^{-a(t)-c} \sigma(t)\dot{v}(t,x)\,dx + \int_{a(t)+c}^{\infty} \sigma(t)\dot{v}(t,x)\,dx + \lim_{R\to\infty}\int_R (\mathbf{T}_R\dot{\mathbf{x}})\cdot d\mathbf{S} = 0, \qquad 0 \leqslant t \leqslant t_V \tag{25}$$

is used in the derivations of eqns (21)–(24) where $R$ is the radius of a semicircle with center located at the coordinate origin.

Equations (22)–(24) show that $E_1$ is the work done by $\sigma(t)$ prior to crack extension, $E_2$ is the work by $\sigma(t)$ during crack extension and $E_3$ is the negative work by $\sigma(t)$ during off-loading after the crack arrests. No energy except for surface energy is consumed during the entire action of $\sigma(t)$. Therefore it results that the term on the left-hand side of eqn (21) is the surface energy per crack tip. Based on eqn (21), the dissipative rate of surface energy $E_s(t)$ for a crack with a single tip can be written as

$$\frac{dE_s(t)}{dt} = \frac{\pi}{E_d}K_d^2(t)\dot{a}(t). \tag{26}$$

Equation (26) is a fundamental formula for analysis of energy balance during fragmentation.

After implementing a series of excellent experiments by using the caustic method combined with the Cranz–Schardin camera system. Arakawa and Takahashi (1991a, b) discovered a very important constant $R^*\dot{a}$, the branching criterion of a propagating crack, defined as

$$R^*\dot{a} = \frac{1}{E_d}(K_{db}^2 - K_{dc}^2)\dot{a}, \tag{27}$$

where $K_{db}$ is the stress intensity factor at the moment the crack branches. However, the physical meaning of $R^*\dot{a}$ seems to be a mystery. The explanation given by them is only based on its unit because it is defined only by experimental data instead of a theoretical analysis.

Comparing eqn (26) with eqn (27), it is apparent that $R^*\dot{a}$ is exactly the increment of the dissipative rate of surface energy, apart from a constant $\pi$ resulting from the definition of stress intensity factor, for a given velocity of crack propagation. Thus in terms of both theoretical and experimental results, the mechanism of crack branching is such that a crack starts branching when the increasing rate of internal energy in the vicinity of a crack tip is greater than the critical value of the dissipative rate of surface energy. This results since more energy needs to be released through formation of new surfaces instead of the extension of a surface of one crack.

The efficiency coefficient for work done during state III is introduced as

$$c_f = \frac{E_s}{E_2} = 1 - \frac{1 + \dfrac{c}{a_0}\left(1 - \dfrac{K_{dc}^2}{K_{da}^2}\right)}{1 + \dfrac{c}{a_0}\left(1 - \dfrac{K_{dc}^2}{K_{da}^2}\right) + \dfrac{2}{K_{da}^2 a_0}\displaystyle\int_{t_{II}}^{t_{IV}} K_d^2(t)\dot{a}(t)\,dt}. \tag{28}$$

For $\dot{a}(t) \leqslant 200$ m s$^{-1}$, including consideration of the effect of geometric dependence of specimens on $\dot{a}(t)$, the equation $K_d(t) \approx K_{dc} \approx K_{da}$ holds for many engineering materials [e.g. see Kanninen and Popelar (1985)]. In this case, eqn (27) gives

$$\tfrac{1}{2}E_t = E_s = \frac{\pi}{E_d}\int_{t_{II}}^{t_{IV}} K_d^2(t)\dot{a}(t)\,dt = \frac{\pi}{E_d}K_{dc}^2 a_0 \tag{29}$$

and then $c_f = 2/3$.

Since eqn (29) is exactly consistent with the result obtained by Griffith (1920) under static conditions, the following conclusion appears to be true. During state III, the surface energy consumed due to formation of new surfaces is transformed from internal energy or strain energy. Under dynamic conditions, the collection of experimental data supporting the assertion can be found in the literature (Kanninen and Popelar, 1985). Thus $c_f = 2/3$ suggests that formation of new surfaces dissipates almost 70% of the work done by external loading during crack extension. In terms of (9)–(11), the other 1/3 of the work is converted to kinetic energy which should contain the part transformed from strain energy due to the relaxation of constraint caused by crack extension.

The solution for a spherically symmetric fluid model obtained by Grady (1982) gives that $E_s = 2/3E_t$ and $E_k = 1/3E_t$. This means that as an exact description of state III, if $\dot{a}(t) \leqslant 200\ \text{m s}^{-1}$, the present result for the energy ratio is in exact agreement with Grady's result. Recent theoretical and experimental results [e.g. Englman *et al.* (1987) and Lankford and Blanchard (1991)] are in agreement with the Grady model.

More general cases are analysed in the following. For simplicity without loss of generality, the body force is ignored in the derivation. In order to measure the general nature of surface energy resulting from inhomogeneity and anisotropy of materials, based on eqn (21) or (26), the surface energy under three-dimensional conditions is defined by

$$E_s(t) = \int_{t_{II}}^{t} dt \int_{S_f(N,t)} \frac{\partial\gamma(\dot{s}, K_{dg})}{\partial t}\,ds, \qquad K_{dg} = K_{dg}(\mathbf{X}, \alpha, t) \quad t_{II} \leqslant t \leqslant t_{IV}, \tag{30}$$

where $\gamma$ denotes the density of surface energy at the point $\mathbf{X}$ with the normal $\alpha = \alpha(\mathbf{X}, t)$ on the fractured surface, $\dot{s}$ is the velocity of surface extension of the crack, $S_f$ is the fractured area of a fragment and $K_{dg}$ is the generalized stress intensity factor with inhomogeneous and anisotropic properties during crack propagation. Theoretically speaking, for a homogeneous and isotropic material one has $K_{dg}(\mathbf{X}, \alpha, t) = K_d(t)$ and the dissipative rate of surface energy is of the form

$$\int_{S_f(N,t)} \frac{\partial\gamma(\dot{s}, K_{dg})}{\partial t}\,ds = \int_{S_f(N,t)} \frac{d\gamma(\dot{s}, K_d)}{dt}\,ds = \int_{S_f(N,t)} \dot{s}\frac{d\gamma(\dot{s}, K_d)}{ds}\,ds = \dot{s}\gamma(\dot{s}, K_d). \tag{31}$$

Here $\dot{s}$ and inertial effects on $K_d$ are assumed to be uniform for each portion of the entire fracture surface. Substitution of (31) into (30) leads to

$$E_s(t) = \int_{t_{II}}^{t} \gamma(\dot{s}, K_d)\dot{s}\,dt. \tag{32}$$

Equation (32) has the same form as (21) or (26). It turns out from (32) that even for crack extension with low velocity, neglecting effects of inhomogeneity and orientation, the surface energy may not be a linear function of surface area. This is one of the complex characteristics in the analysis of fragmentation of composite materials. For a homogeneous and isotropic material with $\dot{s} \leqslant 200\ \text{m s}^{-1}$, $\gamma(\dot{s}, K_d) = \gamma_0$ is a constant. This means that the surface energy $E_s(S_F) = \gamma_0 S_F$ is a linear function of the fracture surface $S_F$ which provides an indentity $S_{F_{i+1}}E_s(S_{F_i}) = E_s(S_{F_{i+1}})S_{F_i}$ between two arbitrary fragments with the surface areas $S_{F_i}$ and $S_{F_{i+1}}$.

Based on the preceding analysis, crack extension is presently considered to be possible if and only if the input energy causes the strain energy in the crack tip region to be greater than or at least equal to a certain value. In other words, the strain energy must be in the

Table 1. Transformation of strain energy into surface energy

| $E_s/\Delta E_i$ | Materials | Specimens | $\dot{a}$ (m s$^{-1}$) | Authors and date |
|---|---|---|---|---|
| 1.04 | Homalite-100 | M-CT | <250 | Kobayashi *et al.* (1980) |
| 0.98 | Polycarbonate | M-CT | <500 | Kobayashi *et al.* (1980) |
| 0.97 | — | DCB | 104 | Kanninen and Popelar (1985) |
| 0.98 | Araldite | DCB | 180 | Kanninen and Popelar (1985) |

critical state of dynamic equilibrium and an increment of strain energy on dynamic equilibrium is consumed by surface energy during crack extension. Actually the energy determined by eqn (23) is exactly the part which is greater than the critical value. The mathematical expression of this statement is given from eqns (10) or (15) and (30) by

$$E_s = \int_{t_{II}}^{t_{IV}} dt \int_{S_f(\aleph,t)} \frac{\partial \gamma(\dot{s}, K_{dg})}{\partial t}\, ds = \int_{t_{II}}^{t_{IV}} dt \int_{\chi(\aleph,t)} \mathrm{tr}(\mathbf{TD})\, dv = \int_{t_{II}}^{t_{IV}} dt \int_{\kappa(\aleph)} \mathrm{tr}(\mathbf{T}_R^T \dot{\mathbf{F}})\, dV. \quad (33)$$

The strain energy stored is considered to be converted into other forms in the following two manners: (1) it is dissipated by overcoming the negative work done by off-loading as indicated in eqn (24); (2) it is transformed into kinetic energy due to relaxation of constraints on the boundaries of the fragment caused by crack extension. Equation (33) is hereafter called the field equation for formation of a fragment.

The experimental data listed in Table 1 is the ratio of surface energy to the decrease $\Delta E_i$ of strain energy at the moment of crack arrest, obtained by Kobayashi *et al.* (1980) and Kanninin and Popelar (1985). The proximity of this ratio to one is in agreement with the fundamental assumptions noted earlier in the theoretical analysis.

Obviously, it still is a difficult task employing eqn (33) to make quantitative analysis of fragmentation because state III is involved in a series of almost formidable topics for initial and boundary value problems. For the sake of brief discussion, based on eqn (33), a simplified model is introduced in the following.

It is an acceptable assumption (even for the occurrence of large deformation at state II) that deformation is infinitesimal for state III because the material has reached its limit state. In this circumstance, $\mathbf{x}$, $\chi$ and $\alpha$ become

$$\mathbf{x} = \chi_\kappa(\mathbf{x}, t_{II}), \qquad \alpha = \alpha(\mathbf{X}, t_{II}) \qquad \text{and } \chi(\aleph, t) = \chi(\aleph, t_{II}), \quad (34)$$

for $t_{II} \leqslant t \leqslant t_{IV}$. In terms of (34), the field equation (33) becomes

$$E_s(t) = \int_{\chi(\aleph, t_{II})} dv \int_{t_{II}}^{t} \mathrm{tr}(\mathbf{TD})\, dt, \qquad t_{II} \leqslant t \leqslant t_{IV}. \quad (35)$$

The term tr(**TD**) is expanded at $t = t_{II}$ as a Taylor series

$$\mathrm{tr}(\mathbf{TD}) = P_{II} + \frac{\partial P_{II}}{\partial t}(t - t_{II}) + \frac{1}{2!}\frac{\partial^2 P_{II}}{\partial t^2}(t - t_{II})^2 + \cdots \quad (36)$$

where $P_{II}$ is introduced for convenience as follows:

$$\mathrm{tr}(\mathbf{TD})|_{t_{II}} = P_{II} = P_{II}(\mathbf{x}, t_{II}) \quad \text{and} \quad \left.\frac{\partial^n \mathrm{tr}(\mathbf{TD})}{\partial t^n}\right|_{t_{II}} = \frac{\partial^n P_{II}}{\partial t^n}, \qquad (n = 1, 2, \ldots). \quad (37)$$

Substitution of (36) into (35) leads to

$$E_s(t) = (t-t_{II})\int_{\chi(\aleph,\,t_{II})} P_{II}\,dv + \tfrac{1}{2}(t-t_{II})^2\int_{\chi(\aleph,\,t_{II})}\frac{\partial P_{II}}{\partial t}\,dv + \frac{1}{3\cdot 2!}(t-t_{II})^3\int_{\chi(\aleph,\,t_{II})}\frac{\partial^2 P_{II}}{\partial t^2}\,dv + \cdots. \quad (38)$$

The physical meaning of $E_s(t)$ implies that the series expansion (38) is convergent. $E_s(t)$ is an increasing function of $t$ for $t_{II} < t < t_{IV}$, i.e. $dE_s(t)/dt > 0$ ($t_{II} < t < t_{IV}$). As $t = t_{IV}$, $E_s(t)$ reaches an extreme value, a maximum, which implies

$$\left.\frac{dE_s(t)}{dt}\right|_{t=t_{IV}} = \int_{\chi(\aleph,\,t_{II})} P_{II}\,dv + \Delta t_{III}\int_{\chi(\aleph,\,t_{II})}\frac{\partial P_{II}}{\partial t}\,dv + \frac{1}{2!}(\Delta t_{III})^2\int_{\chi(\aleph,\,t_{II})}\frac{\partial^2 P_{II}}{\partial t^2}\,dv + \cdots = 0 \quad (39)$$

and

$$\left.\frac{d^2E_s(t)}{dt^2}\right|_{t=t_{IV}} = \int_{\chi(\aleph,\,t_{II})}\frac{\partial P_{II}}{\partial t}dv + \Delta_{III}\int_{\chi(\aleph,\,t_{II})}\frac{\partial P_{II}}{\partial t^2}\,dv + \cdots < 0, \quad (40)$$

with $\Delta t_{III} = t_{IV} - t_{II}$. It follows from (39) that $\Delta t_{III}$ is controlled by the stress state, the strain rate and the geometric parameters of a fragment and its value reflects a series of dynamic characteristics of the fragmentation process. $dE_s(t)/dt > 0$ ($t_{II} < t < t_{IV}$) and (40) are two important constraint conditions for this model. After $\Delta t_{III}$ is calculated by use of eqn (39), the surface energy dissipated by formation of a fragment is given from eqn (38) as

$$E_s(S_F)|_{t=t_{IV}} = \Delta t_{III}\int_{\chi(\aleph,\,t_{II})} P_{II}\,dv + \tfrac{1}{2}(\Delta t_{III})^2\int_{\chi(\aleph,\,t_{II})}\frac{\partial P_{II}}{\partial t}\,dv + \frac{1}{3\cdot 2!}(\Delta t_{III})^3\int_{\chi(\aleph,\,t_{II})}\frac{\partial^2 P_{II}}{\partial t^2}\,dv + \cdots. \quad (41)$$

The physical meaning of eqn (41) is that the incremental loss of strain energy from a fragment during state III is consumed by surface energy.

When the volume $V = \chi(\aleph, t_{II})$ of a fragment is very small, one might assume that $P_{II}$ and $(\partial^n P_{II}/\partial t^n)$ are constants within the fragment, and the first three terms of eqn (39) are truncated for calculation of $t_{IV}$. In this case, $\Delta t_{III}$ is determined by

$$\Delta t_{III} = \left(\frac{\partial^2 P_{II}}{\partial t^2}\right)^{-1}\left[-\frac{\partial P_{II}}{\partial t} \pm \sqrt{\left(\frac{\partial P_{II}}{\partial t}\right)^2 - 2P_{II}\frac{\partial^2 P_{II}}{\partial t^2}}\right] > 0. \quad (42)$$

This equation should satisfy conditions $dE_s(t)/dt > 0$ ($t_{II} < t < t_{IV}$) and (40) as constraints on the approximation. For a homogeneous isotropic material and $\dot{s} < 200$ m s$^{-1}$, the first three terms of eqn (41) yield

$$\frac{S_F}{V} = \frac{1}{\gamma_0}\left[\Delta t_{III}P_{II} + \frac{1}{2}(\Delta t_{III})^2\frac{\partial P_{II}}{\partial t} + \frac{1}{3\cdot 2!}(\Delta t_{III})^3\frac{\partial^2 P_{II}}{\partial t^2}\right] \quad (43)$$

with $E_s = \gamma_0 S_F$ and $\Delta t_{III}$ given by (42). Theoretically speaking when the physical parameters on the right-hand side of eqn (43) are known the geometric parameters (the surface $S_F$ and the volume $V$ of its left-hand side) can also be determined. However, so far the discussion on fragmentation has not provided any information about the shape of a fragment or the fracture pattern of the entire fragmentation process in part because there are infinite solutions to $S_F$ for a given $V$ or infinite solutions to $V$ for a given $S_F$. It follows that it is

necessary for the complete description of fragmentation to examine the principles relevant to the geometric configuration of fragmentation. This is the topic of the next section.

## 3. GEOMETRIC CONSTRAINTS

The goal of this section is to show that deterministic geometric constraints exist during fragmentation and play an important role in geometric analysis of crack networks and the prediction of favorite shapes for fragments. The following discussion contains two aspects: global and local constraints.

### 3.1. *Global constraint*

For any finite solid body with arbitrary shape, its curved boundary surface can be categorized by Euler's constant (Blackett, 1967; Meyerhoff, 1992). Euler's constant remains invariant for the surfaces of two bodies provided that one is homoemophic to the other. In other words, it depends only on the topological structure of a closed surface. Mathematically speaking, the crack network formed during fragmentation on the surface of a body is a subdivision of this surface into a polyhedron. Therefore, the geometric parameters of all fragments on the closed surface obey the Euler theorem

$$\chi_E = N_0 - N_1 + N_2, \tag{44}$$

where $\chi_E$ is the Euler characteristic, $N_0$ is the number of crack junctions on the fracture surface, $N_1$ is the number of cracks and $N_2$ the number of all fragments. The value of $\chi_E$ varies with the characteristic of the surface. In particular, $\chi_E$ (sphere) = 2, $\chi_E$ (torus) = 0 and $\chi_E$ (two holed torus) = $-2, \ldots,$ $\chi_E$ ($n$-holed torus) = $2-2n$ (Meyerhoff, 1992). Several applications are introduced below.

From the idealistic point of view, fragmentation of a spherical shell subjected to uniform internal pressure is expected to produce fragments with the identical size, shape and with the same number of cracks emanating from each vertex since both the geometric and physical conditions are spherically symmetric. Fragmentation of a spherical shell in this manner corresponds to a regular subdivision in a topological sense. A subdivision of a surface into a polyhedron is regular if each face has the same number of edges and each vertex has the same order (Blackett, 1967). The order of a vertex is the number of times the vertex appears as the end of an edge.

Constrained by a regular subdivision, $N_0$, $N_1$ and $N_2$ are related by

$$jN_0 = 2N_1, \qquad kN_2 = 2N_1, \tag{45}$$

where $k$ and $j$ mean that the faces of a regular subdivision have $k$ edges and the vertices are each of order $j$. After substitution of (45) into (44), eqn (44) is simplified to

$$\chi_E = \left(\frac{2}{j} - 1 + \frac{2}{k}\right) N_1. \tag{46}$$

For a sphere, (46) gives

$$N_0 = \frac{4k}{2(k+j) - jk}, \tag{47}$$

$$N_1 = \frac{2jk}{2(k+j) - jk}, \tag{48}$$

$$N_2 = \frac{4j}{2(k+j)-jk}. \tag{49}$$

All the solutions to eqns (47)–(49) for a sphere are listed as follows:

$$\text{(i)} \begin{pmatrix} N_0 \\ N_1 \\ N_2 \end{pmatrix} = \begin{pmatrix} k \\ k \\ 2 \end{pmatrix}_{j=2,\, k=N_1}, \qquad \text{(ii)} \begin{pmatrix} N_0 \\ N_1 \\ N_2 \end{pmatrix} = \begin{pmatrix} 2 \\ j \\ j \end{pmatrix}_{j=N_1,\, k=2},$$

$$\text{(iii)} \begin{pmatrix} N_0 \\ N_1 \\ N_2 \end{pmatrix} = \begin{pmatrix} 4 \\ 6 \\ 4 \end{pmatrix}_{j=3,\, k=3}, \qquad \text{(iv)} \begin{pmatrix} N_0 \\ N_1 \\ N_2 \end{pmatrix} = \begin{pmatrix} 8 \\ 12 \\ 6 \end{pmatrix}_{j=3,\, k=4},$$

$$\text{(v)} \begin{pmatrix} N_0 \\ N_1 \\ N_2 \end{pmatrix} = \begin{pmatrix} 6 \\ 12 \\ 8 \end{pmatrix}_{j=4,\, k=3}, \qquad \text{(vi)} \begin{pmatrix} N_0 \\ N_1 \\ N_2 \end{pmatrix} = \begin{pmatrix} 20 \\ 30 \\ 12 \end{pmatrix}_{j=3,\, k=5},$$

$$\text{(vii)} \begin{pmatrix} N_0 \\ N_1 \\ N_2 \end{pmatrix} = \begin{pmatrix} 12 \\ 30 \\ 20 \end{pmatrix}_{j=5,\, k=3}.$$

Solution (i) here is a trivial case. Solutions (ii)–(vii) are illustrated in Fig. 3. Note that the definition of a regular subdivision does not have any requirement on the size and shape of a fragment appearing on the surface of a sphere. A solution with practical interest needs to

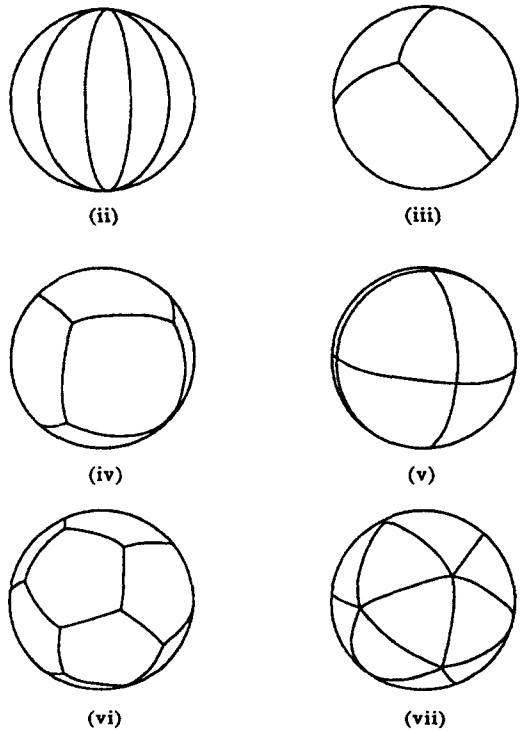


Fig. 3. Six regular subdivisions of a spherical shell given by Euler's equation.

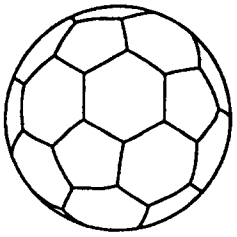

Fig. 4. An irregular subdivision of a spherical shell.

have a determinable dimension. Here the limitation on the surfaces of fragments is that the size and shape of each surface is identical to one another.

One of the most significant properties of a regular subdivision for a sphere is that since both $N_0 > 2$ and $N_2 > 2$ a finite number of solutions (actually five) for $N_0$, $N_1$ and $N_2$ exist. Solutions (iii)–(vii) illustrate that because of the constraint of the Euler constant, if a spherically symmetric condition holds until the moment of fragmentation of a sphere, fragmentation at that moment will only produce at most 20 fragments. If $N_2 > 20$, fragments with uniform size and shape will never appear during fragmentation of a spherical shell subjected to uniform deformation. In real fragmentation processes defects in materials, errors in manufacture and variations of loading influence the ideal symmetry. Therefore, non-uniform local fracture affects the fragmentation patterns. Two other possibilities are that (a) the initial fracture pattern is controlled by the regular subdivision and then a multiple fracture process takes place in the subsequent stages; (b) the vertices which serve as crack sources are regular but fragments are not regular. An example of case (b) is shown in Fig. 4. Here note that each vertex is identical while some fragments have six edges and others (12 pieces) have five edges. In the experimental photographs achieved by Slate *et al.* (1967), visible parts of the instantaneous crack network on a spherical shell of hard copper beryllium have a consistent pattern with case (b) under internal blast pressure.

When $\chi_E$ is replaced by zero which stands for a torus, the result of eqn (46) for the regular subdivision is substantially different from the result of a sphere. In fact, (44) and (45) lead to

$$\chi_E = \left(\frac{2}{j} - 1 + \frac{2}{k}\right) N_1 = 0, \tag{50}$$

which shows that an infinite number of polygons (subdivisions) exist for $N_0$, $N_1$ and $N_2$ corresponding to three cases of $j$ and $k$ ($k = 3$, $j = 6$; $k = j = 4$; $k = 6$, $j = 3$). An example for $j = k = 4$ is illustrated in Fig. 5. This implies that the uniform fragmentation of a torus has a less restricting constraint as compared to a sphere since the number of polygons is

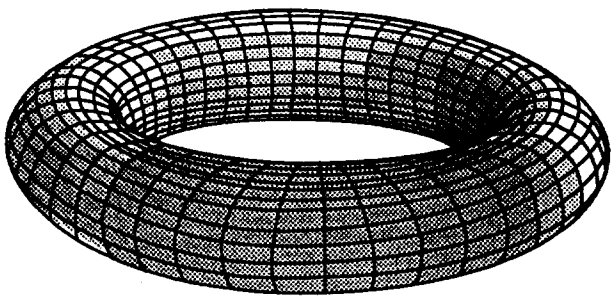

Fig. 5. A regular subdivision of a torus given by Euler's equation.

not limited. Figure 6 is an experimental result which demonstrates the global constraint on uniform plane fragmentation and is based on solution $j = k = 4$. This experiment was conducted using the following procedures:

- heat a glass plate gradually to 900°F;
- hold the plate for 1 hr at this temperature;
- decrease the temperature gradually to 750°F;
- rapidly cool the plate in water.

It is evident from this figure that the geometric constraints on plane fragmentation are in perfect agreement with the theoretical predictions. The plane fragmentation as shown in Fig. 6 is consistent with Fig. 5 since the subdivision of a torus is equivalent to the subdivision of a plane. Hence the idealized model is directly applicable to physical fragmentation problems.

In evaluating the surface energy, the size and shape of fragments, and other parameters produced by fragmentation of a shell, it could be very significant to analyse the global constraint. Al-Hassani and Johnson (1969), Johnson (1972) and Kobelev (1990) seemed to be unaware of the special constraints on fragmentation of a spherical shell, so there are several unreasonable assumptions in their papers. Kobelev (1990) assumed that the shapes of fragments are circular and rectangular corresponding to uniform internal pressure. Both shaped are incompatible with respect to the global energy field (assuming the fragment number $N_2 > 6$). In fact, it will be shown below that a circular fragment is the least probable shape.

When a point load with a moderate speed acts on an untempered glass plate or shell of arbitrary shape, even for general boundary constraints, the fracture pattern caused by the impact always consists of a group of radial cracks with possible secondary "ring" cracks which converge towards the loading point as shown in Fig. 7. Careful observation indicates that the radial cracks divide the region close to the loading point into almost equal geometric parts. This common phenomenon which can be seen everywhere is not limited to brittle materials. Similar fracture patterns for ductile materials such as copper, aluminum and lead are also produced when geometric and loading conditions are symmetric (Ghosh and Travis, 1979). It is difficult to explain the fragmentation process in detail using traditional ideas. In this case, the regular subdivision (ii) shown in Fig. 3 gives a reasonable illustration. The vertex of the faces of subdivision (ii) corresponds to the loading point, the region near the loading point is a portion of a sphere. Under the constraint of the Euler characteristic, the possible subdivision only allows the radial crack pattern. As a matter of result, this is an ideal example of the global constraint because the energy field completely matches with the fracture pattern.

### 3.2. *Local constraint*

When material constants of a medium are given, a key geometric parameter for calculation of surface energy is the fracture surface area of a fragment. The essential step

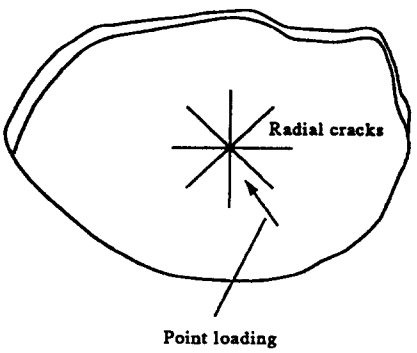


Fig. 7. A crack network on the solid surface caused by a point loading.

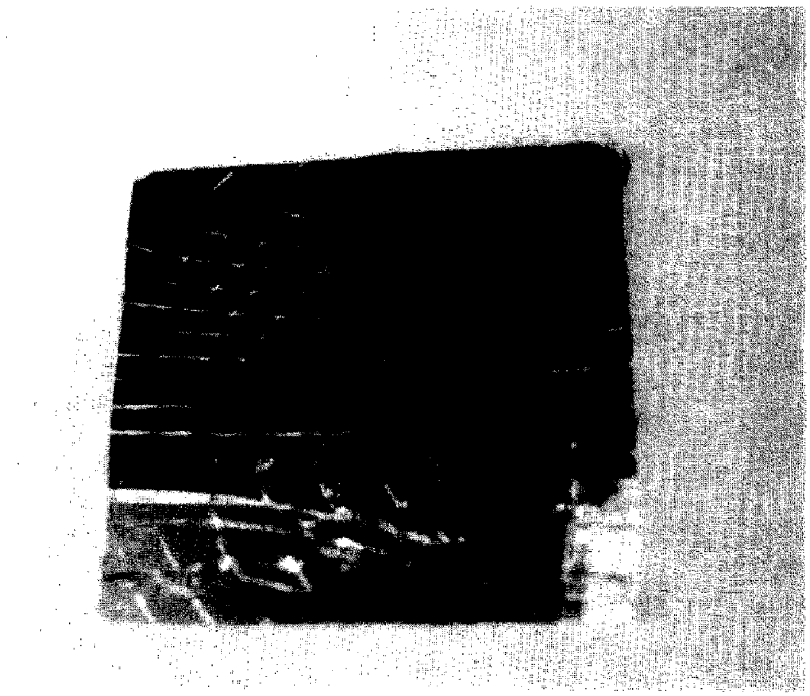

Fig. 6. Uniform fragmentation of a glass plate.

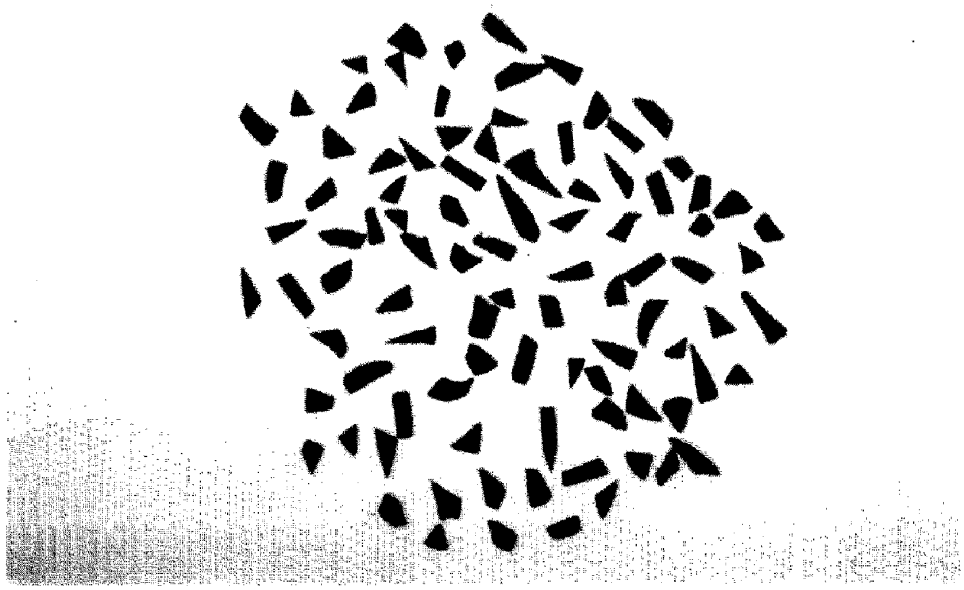

Fig. 8. Small fragments of a thin glass shell.

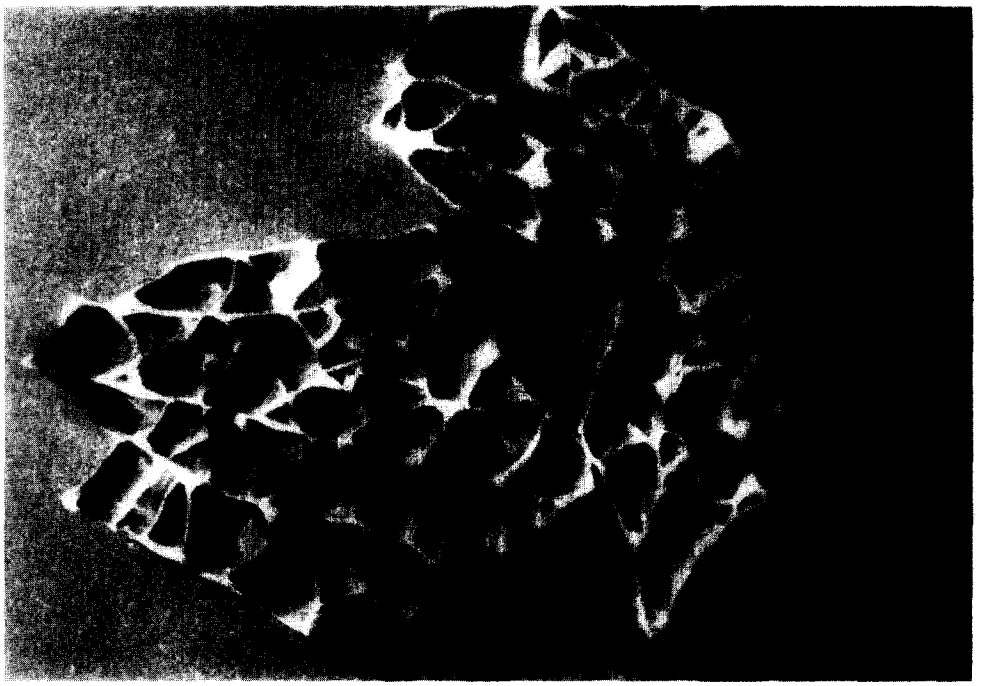

Fig. 10. Crack networks of a glass plate with three layers.

for this is to find the shape of the fragment. As indicated in the above section, classical approaches will encounter great difficulties in treating the problem. In the present work, principles of energy consumption are applied to analyse possible geometric constraints on the shape of the homoemorphic family of a fragment at a local level.

The mass or volume of a fragment can be easily measured with the use of ordinary instruments. Therefore emphasis here is placed on calculation of the surface area of a fragment with a given volume. The surface area corresponding to a given volume has infinitely many values which, mathematically speaking, consists of a group of homeomorphisms to a spherical surface. The interest for quantitative analysis of fragmentation is the extreme value of the surface area. This is a classical variational problem. It is easy to prove that the surface area with a given volume does not have a maximum unless more constraints are specified and hence only the minimum of the surface area is available through a direct variational approach.

For a two-dimensional problem relevant to fragmentation of thin plates with uniform thickness, the length of the perimeter which stands for fracture surface area is the desired parameter. Under polar coordinates, the minimum perimeter with a given area is determined by minimizing the integral

$$I = \int \sqrt{(\mathrm{d}r)^2 + (r\,\mathrm{d}\theta)^2} + \lambda \int \tfrac{1}{2} r^2\,\mathrm{d}\theta - \int (c_1\,\mathrm{d}r + c_2\,\mathrm{d}\theta), \tag{51}$$

where $\lambda$ is the Lagrangian multiplier and $c_1$, $c_2$ are the constants of boundary constraints. The condition $(\partial I/\partial\theta) = (\partial I/\partial(\mathrm{d}\theta)) = 0$ (Kimbal, 1952) gives the differential equation

$$\frac{\mathrm{d}\theta}{\mathrm{d}r} = \frac{2c_2 - \lambda r^2}{r\sqrt{4r^2 - (2c_2 - \lambda r^2)^2}}. \tag{52}$$

Without loss of generality, $c_2$ is taken as zero for convenience, and the solution to (52) is of the form

$$r = \left| \frac{2}{\lambda} \cos(\theta - \alpha_0) \right|, \tag{53}$$

where $\alpha_0$ is the integral constant. Equation (53) is the polar equation of a circle with the radius $1/\lambda$. Its physical meaning for fragmentation of a plate is that, of fragments with a given area, a circular fragment dissipates the minimum internal energy because of the minimum fracture surface. For a more elaborate investigation, the perimeter $L$ of a regular polygon with a given area $A$ and $N_1$ edges of equal length is written in the form

$$L = \sqrt{4N_1 \tan\frac{\pi}{N_1}}\sqrt{A}, \qquad (N_1 \geqslant 3). \tag{54}$$

Note that $L$ is a descending function of $N_1$. When $N_1 = 3$, $L$ has the maximum $L_{\max} = \sqrt{12\sqrt{3}}\sqrt{A}$ and when $N_1 \to \infty$ $L$ tends to the minimum $L_{\min} = \sqrt{4\pi}\sqrt{A}$, and their ratio is $L_{\max}/L_{\min} = 1.286$ or $L_{\min}/L_{\max} = 0.778$. If the material of a fragment is homogeneous and isotropic as well as $\dot{s} < 200$ m s$^{-1}$, combining eqn (54) with eqns (41) and (43) results in

$$\frac{S_F}{V} = \frac{L}{A} = \frac{1}{\sqrt{A}}\sqrt{4N_1 \tan\frac{\pi}{N_1}} = \frac{p_{II\text{-}IV}}{\gamma_0}, \tag{55}$$

with

$$p_{\text{II-IV}} = \Delta t_{\text{III}} P_{\text{II}} + \tfrac{1}{2}(\Delta t_{\text{III}})^2 \frac{\partial P_{\text{II}}}{\partial t} + \frac{1}{3 \cdot 2!}(\Delta t_{\text{III}})^3 \frac{\partial^2 P_{\text{II}}}{\partial t^2} + \cdots. \tag{56}$$

The ratio $r_i = L/\sqrt{A}$ $(i = N_1)$ and the increment $\delta = (r_i - r_{i+1})/r_{i+1}$, varying with the number of edges, are listed in Table 2. This reveals that there are substantial decreases in perimeter length (and hence surface area) as the number of sides increases. It turns out from (55) that when a fragment is small, the surface energy consumed by a fragment with a given area is inversely proportional to the number of its edges.

From the point of view of strength theory, the failure event of a material usually takes place at the moment when the energy stored within a region reaches a critical value, i.e. the highest level. Table 2 illustrates that there are two big jumps between a quadrilateral and a triangle (14%), and between a pentagon and a quadrilateral (4.9%). This implies that a triangle and a quadrilateral are the most favorable shapes (in terms of surface energy absorption) for a small fragment. When $N_1$ is greater than seven, the increment of energy is less than 1% so a small fragment with more than seven edges will not frequently appear during fragmentation, while a circle is the most improbable shape for a fragment. This may be a significant reason why circular fragments are rarely seen. This result illustrates the advantage created by considering a combination of the energy constraint on a fragment in addition to its geometric structure.

To check the theoretical results, a series of experiments and direct observations have been carried out by the authors. In these experiments 15 types of plates and shells of standard window glass, glass bulbs and clay ceramics were taken as the experimental materials and they were each broken into many fragments with different sizes by arbitrary impact loadings. (The impact loading was applied with a standard hammer. The specimens were hit repeatedly with the hammer until the fragments were reduced to a certain size. No attempt was made to quantify the magnitude of this impact force since this result was not needed presently.) The fragments were categorized into four size groups by sieves. Experimental data revealed that when the average mass or volume of each fragment of a group is less than a critical value or, more accurately, a critical band, at least 70% of the fragments in that group had triangular or quadrilateral shapes. Their typical profiles are shown in Fig. 8. It is evident from this photograph that most fragments have three or four edges (triangle or quadrilaterals) and this result is exactly consistent with the prediction in Table 2. In most cases, considering all fragments of different sizes, the maximum number of edges of a fragment was less than seven. No circular fragment ever appeared. Several experimental results are plotted in Fig. 9 where $r_s$ is the percentage of the number of triangular and quadrilateral fragments to the total number of fragments of each group and $\bar{m}$ is the average mass of a fragment. The results convincingly indicate that as the fragment size is reduced, most fragments attain a triangular or quadrilateral geometry.

Further experimental verification of present predictions is shown in Fig. 10 which displays crack network patterns of a fractured glass plate with three layers (safety glass). It is clear that there is no fragment which has more than six sides. It is necessary to point out that this is not an isolated phenomenon, but exists everywhere in fragmentation events.

Table 2. Relation between two-dimensional shape and energy

| $N_1$ | $r_i$ | $\delta$ (%) | Shape |
|---|---|---|---|
| 3 | 4.559 | — | triangle |
| 4 | 4.000 | 14.0 | quadrilateral |
| 5 | 3.812 | 4.9 | pentagon |
| 6 | 3.772 | 2.4 | hexagon |
| 7 | 3.672 | 1.4 | heptagon |
| 8 | 3.641 | 0.8 | octagon |
| 9 | 3.620 | 0.5 | nonagon |
| 10 | 3.605 | 0.4 | decagon |
| infinity | 3.545 | 1.7 | circle |

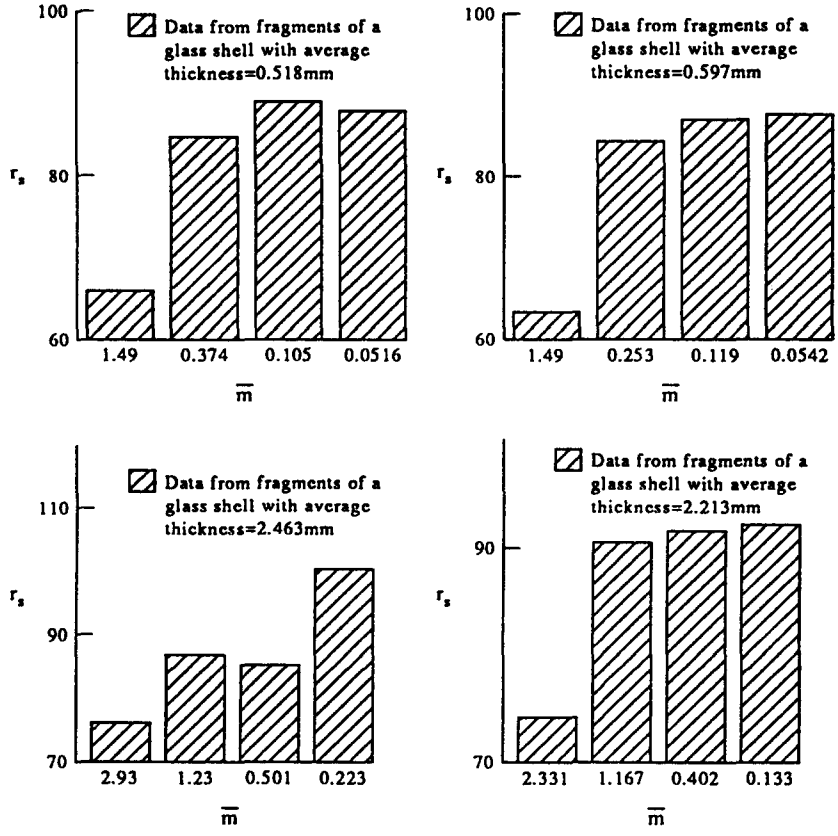


Fig. 9. Experimental results for the ratio of the number of triangular and quadrilateral fragments to the total number of fragments.

Similarly for three-dimensional problems, variational calculations show that the spherical surface is the minimum area for a given volume. The physical meaning is that of all the possible fragments with the same volume, the fragment with a spherical shape consumes the minimum energy. This may be the reason why there exists a unique minimum in the model given by Grady (1982). To compare the spherical surface with surfaces of other shapes, the regular tetrahedron, cube, octahedron, dodecahedron and icosahedron (all of which can be obtained by affine mappings from solutions (iii)–(vii) of Section 3.1) are chosen. The ratio of surface area to (volume)$^{2/3}$ $r_i = S_F/V^{2/3}$ and the increment $\delta = (r_i - r_{i+j})/r_{i+j}$ ($i = N_2$, $j = 2, 2, 4, 8, \infty$) are given in Table 3. Note that the ratio of the maximum to the minimum is equal to $S_{max}/S_{min} = 1.490$. It follows that the general tetrahedron, pentahedron and hexahedron (pentahedron and hexahedron fall between the tetrahedron and cube) are the most probable shapes because of the high jump in energy level. Similarly, the spherical fragment is the most improbable shape. If one picks up any fragment and counts the number of its segment surfaces, the data obtained is in agreement with the theoretical analysis.

Table 3. Relation between three-dimensional shape and energy

| $N_2$ | $r_i$ | $\delta$ (%) | Shape |
|---|---|---|---|
| 4 | 7.206 | — | tetrahedron |
| 6 | 6.000 | 20.1 | cube |
| 8 | 5.719 | 4.9 | octahedron |
| 12 | 5.312 | 7.7 | dodecahedron |
| 20 | 5.148 | 3.2 | icosahedron |
| infinity | 4.836 | 6.4 | sphere |

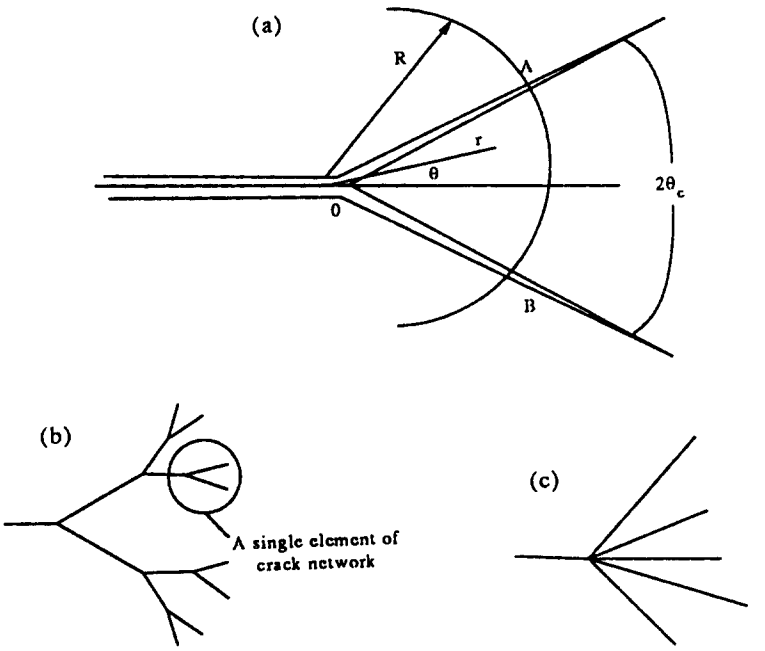


Fig. 11. Three examples of a branching crack. (a) A two-branch crack. (b) The multibranching of a crack. (c) The diverging of a crack.

## 4. AN ILLUSTRATIVE EXAMPLE

To gain a clear physical understanding of the fragmentation mechanism, the modified equation (41) of the general field equation (33) is applied to analyse the branching problem of a two-dimensional crack under quasi-static conditions. For this topic, a large amount of successful experimental data is available for comparison with theoretical analysis [e.g. Schardin (1959) and Arakawa and Takahashi (1991a, b)]. From known experimental results, branching of a single crack may be categorized into three cases: (a) a two-branch crack; (b) a crack network formed by a group of two-branch subcracks; (c) a crack with more than two branches, shown in Fig. 11(a–c), respectively. It is of interest to note that case (b) consists of a chain of case (a) and case (c) is the intensified development of case (a). So case (a) is considered an element of a crack network and it is examined in detail as follows.

A two-branch crack with the symmetric angle $\theta_c$ in Fig. 11(a) is assumed to synchronously originate from a semi-infinite stationary crack embedded in an infinite homogeneous isotropic elastic plate subjected to the dynamic normal point force $f(t)$ per unit width determined by

$$f(t) = f_m \sin\left(\frac{\pi}{2}\frac{t}{t_m}\right), \tag{57}$$

where $f_m$ is the amplitude of $f(t)$, as shown in Fig. 12. In this circumstance, the criterion (26) for the branching of a propagating crack might not readily be adopted because of the simplification of the model. As compensation for this it is straightforward to define that the crack branches as $t = t_{II}$. The fan sector $AOB$ with radius $R$ formed by the two branches of the crack is chosen as a fragment, as illustrated in Fig. 12(a). As the displacement gradient is small, the constitutive equation for the material (Hooke's law) is of the form

$$\mathbf{T}_R = \lambda \,\mathrm{tr}(\mathbf{e})\mathbf{I} + 2\mu\mathbf{e} = \mathbf{T}_R^T, \tag{58}$$

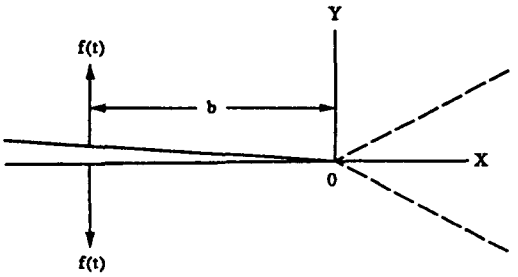


Fig. 12. The model of a branching crack.

where **e** is the infinitesimal strain tensor, and $\lambda$ and $\mu$ are the Lamé constants. Using eqn (58) and $\mathrm{tr}(\mathbf{T}_R^{\mathrm{T}}\dot{\mathbf{F}}) = \mathrm{tr}(\mathbf{T}_R\dot{\mathbf{e}})$, one can obtain

$$\int_{\chi(S,t)} \mathrm{tr}(\mathbf{TD})\,\mathrm{d}v = \int_{\kappa(S)} \mathrm{tr}(\mathbf{T}_R\dot{\mathbf{e}})\,\mathrm{d}V. \tag{59}$$

It follows from (59) that as the deformation is small $\mathrm{tr}(\mathbf{TD})$ can be replaced by $\mathrm{tr}(\mathbf{T}_R\dot{\mathbf{e}})$ in eqns (36)–(41) without any influence on the result. For a plane stress problem, $\mathrm{tr}(\mathbf{T}_R\dot{\mathbf{e}})$ is written from (58) as

$$\mathrm{tr}\,(\mathbf{T}_R\dot{\mathbf{e}}) = \frac{1}{E}[\sigma_{xx}\dot{\sigma}_{xx}+\sigma_{yy}\dot{\sigma}_{yy}-\nu(\sigma_{xx}\dot{\sigma}_{yy}+\sigma_{yy}\dot{\sigma}_{xx})+2(1+\nu)\sigma_{xy}\dot{\sigma}_{xy}], \tag{60}$$

where $T_{ij} = \sigma_{ij}$ $(i, j = x, y)$, $E$ is the elastic modulus and $\nu$ is the Poisson ratio.

Before the crack branches, the stress and strain field can be determined by the complex Westergaard function which is of the form (Irwin, 1957)

$$Z_{\mathrm{I}} = \frac{f(t)}{\pi}\frac{1}{z+b}\sqrt{\frac{b}{z}}, \tag{61}$$

where $z = x+\mathrm{i}y = r(\cos\theta+\mathrm{i}\sin\theta)$. The effect of the stress intensity factor $K_{\mathrm{II}}$ for Mode II on the extension of each branch is ignored here for conciseness of discussion. In fact, the latest results by Isida and Noguchi (1992) reveal that for a symmetric two-branch crack, at the branch tip the stress intensity factor of Mode I is the dominant one for branching angles $2\theta_c \leqslant 60°$. Inserting $\sigma_{yy} = \mathrm{Re}Z_{\mathrm{I}}+y\,\mathrm{Im}\,(\mathrm{d}Z_{\mathrm{I}}/\mathrm{d}z)$, $\sigma_{xx} = \mathrm{Re}Z_{\mathrm{I}}-y\,\mathrm{Im}\,(\mathrm{d}Z_{\mathrm{I}}/\mathrm{d}z)$ and $\sigma_{xy} = -y\,\mathrm{Re}\,(\mathrm{d}Z_{\mathrm{I}}/\mathrm{d}z)$ into (60) leads to

$$\mathrm{tr}(\mathbf{T}_R\dot{\mathbf{e}}) = \frac{2}{E\pi^2}\frac{b}{R}\frac{J(r,\theta)}{Rr}f(t)\dot{f}(t), \tag{62}$$

with

$$J(r,\theta) = \frac{1}{R_{r\theta}^2}\left[(1-\nu)\left(\frac{r}{R}\cos\frac{3}{2}\theta+\frac{b}{R}\cos\frac{\theta}{2}\right)^2+(1+\nu)\left(2\frac{r^2}{R^2}+\frac{r}{R}\frac{b}{R}\cos\theta+\frac{1}{4}R_{r\theta}\right)\sin^2\theta\right], \tag{63}$$

$$R_{r\theta}^2 = \left(\frac{r}{R}\right)^2+2\frac{r}{R}\frac{b}{R}\cos\theta+\left(\frac{b}{R}\right)^2. \tag{64}$$

Corresponding to eqns (36) and (59), eqn (62) produces

$$\left.\frac{\partial^n \operatorname{tr}(\mathbf{T}_R \dot{\mathbf{e}})}{\partial t^n}\right|_{t=t_{II}} = \frac{\partial^n P_{II}}{\partial t^n} = \frac{2}{E\pi^2}\frac{b}{R}\frac{J(r,\theta)}{Rr}\frac{\mathrm{d}^n(f_{II}\dot{f}_{II})}{\mathrm{d}t^n} \qquad (n = 0, 1, 2, \ldots), \tag{65}$$

where

$$\frac{\mathrm{d}^n(f_{II}\dot{f}_{II})}{\mathrm{d}t^n} = \left.\frac{\mathrm{d}^n[f(t)\dot{f}(t)]}{\mathrm{d}t^n}\right|_{t=t_{II}}. \tag{66}$$

Substitution of eqn (65) into (39) leads to

$$\left.\frac{\mathrm{d}E_s(t)}{\mathrm{d}t}\right|_{t=t_{IV}} = \frac{2}{E\pi^2}\frac{b}{R}\left[f_{II}\dot{f}_{II} + \Delta t_{III}\frac{\mathrm{d}(f_{II}\dot{f}_{II})}{\mathrm{d}t} + \frac{1}{2!}(\Delta t_{III})^2\frac{\mathrm{d}^2(f_{II}\dot{f}_{II})}{\mathrm{d}t^2} + \cdots\right]\int_{-\theta_c}^{\theta_c}\mathrm{d}\theta\int_0^R J(r,\theta)\frac{\mathrm{d}r}{R} = 0. \tag{67}$$

Note that in eqn (67) $\chi(\aleph, t_{II}) = \kappa(\aleph)$ is replaced by the area: $-\theta_c \leqslant \theta \leqslant \theta_c$, $0 \leqslant r \leqslant R$. Equation (67) is truncated after three terms to evaluate $\Delta t_{III}$ as

$$\Delta t_{III} = \frac{t_m}{\pi \sin\left(\dfrac{\pi t_{II}}{t_m}\right)}\left[\cos\left(\frac{\pi t_{II}}{t_m}\right) + \sqrt{1+\sin^2\left(\frac{\pi t_{II}}{t_m}\right)}\right]. \tag{68}$$

The positive sign is reasonable for the present analysis. If the velocity of crack propagation is low, the surface energy contributed by the fragment during the branching is given as

$$E_s(t_{IV}) = \frac{\pi}{E}K_{dc}^2 R. \tag{69}$$

In light of eqns (65) and (69), eqn (41) gives

$$R = \frac{2}{\pi^3 K_{dc}^2}\frac{b}{R}\left[\Delta t_{III} f_{II}\dot{f}_{II} + \frac{(\Delta t_{III})^2}{2}\frac{\mathrm{d}(f_{II}\dot{f}_{II})}{\mathrm{d}t} + \frac{(\Delta t_{III})^3}{6}\frac{\mathrm{d}^2(f_{II}\dot{f}_{II})}{\mathrm{d}t^2}\right]\int_{-\theta_c}^{\theta_c}\mathrm{d}\theta\int_0^R J(r,\theta)\frac{\mathrm{d}r}{R}. \tag{70}$$

The formation of a two-branch crack is a special consequence because it requires that the new surfaces formed by the two branches are just sufficient to consume the extra part of the energy over what is needed for extension of a single crack. This special characteristic should be reflected in some physical parameters, such as $\Delta t_{III}$.

As $t_{II} = t_m$, eqn (68) provides $\Delta t_{III} = 0$, and then eqn (70) gives $R = 0$. It follows that if the maximum loading is only large enough to drive a crack to the critical branching state then the extension of the crack may be self-similar or may cause an unsuccessful bifurcation. It results from the meaning of $t_{II} = t_m$ that after a crack starts branching, if $\Delta t_{III} = t_m - t_{II}$ or $t_{IV} = t_m$, then the branching crack arrests due to the energy constraint controlled by the external loadings. The solution of eqn (68) for the condition $t_{IV} = t_m$ is a specific value given by $t_{II}/t_m = 0.3381$. A set of known experimental data listed in Table 4 also consistently

Table 4. Experimental data of ratio $t_{II}/t_{IV}$

| No. | $t_{II}$ ($\mu s$) | $t_{IV}$ ($\mu s$) | $t_{II}/t_{IV}$ | $\theta_c$ (degree) | Materials | Authors and date |
|---|---|---|---|---|---|---|
| 1 | 102 | 212 | 0.4811 | 53.4 | Homalite-100 | Ramulu *et al.* (1984a,b) |
| 2 | 83 | 174 | 0.4770 | 8 | Polycarbonate | Ramulu and Kobayashi (1985) |
| 3 | 70 | 150 | 0.4667 | ~60 | Homalite-100 | Arakawa and Takahashi (1991a) |
| 4 | 77 | 189 | 0.4074 | ~60 | Homalite-911 | Arakawa and Takahashi (1991b) |
| 5 | 98 | 196 | 0.5000 | ~52 | Epoxy | Arakawa and Takahashi (1991b) |

exhibits that $t_{II}/t_m$ seems to be a constant for the two-branch crack. The error between theoretical and experimental results is mainly attributed to the simplification of the model which considers an approximate quasi-static stress and strain field instead of the real dynamic field of a propagating crack, and to the neglect of the effects of shear stress on the branched cracks. However, the simplification in the analysis here does not cause any large deviation from experimental results. The constraint conditions $dE_s(t)/dt > 0$ ($t_{II} < t < t_{IV}$) and (40) hold for this illustrative example.

When $\Delta t_{III} < t_m - t_{II}$ or $t_{II} > 0.3381 t_m$, each of the two branches of the crack would be driven by external loadings lower than the maximum value $f_m$ to produce two or more new branches so that a multibranching crack network may form as shown by the experimental photographs given by Schardin (1959) and Ewalds and Wanhill (1985). In addition, $\Delta t_{III} > t_m - t_{II}$ or $t_{II} < 0.3381 t_m$ is the other important case which may lead to confusion without careful analysis. In fact, the high rate of energy input caused by the high loading rate needs to be balanced by the formation of more than two new surfaces. Therefore when an analytical model is limited to a two branch crack, the branching time $t_{IV}$ should naturally be greater than the maximum time $t_m$ of the model. Hence there may be two possibilities concerning the ratio $t_{II}/t_m$ for diverging cracks from a single source. First, $t_{II}/t_m < 0.3381$ still holds for the divergence. This case is recorded by Arakawa and Takahashi (1991b). In their experiments, when the branches of an extension crack are more than three, $t_{II}/t_m = 0.1482$ is much less than the uniform average value of $t_{II}/t_m = 0.4664$ for the two-branch cracks listed in Table 4. The second case is that the ratio remains unchanged but the branches of a crack are more than two. In summary, the higher the loading rate, the larger the number of branches of a crack.

Having discussed that eqn (70) holds only for $t_{II} = 0.3381\ t_m$ or $t_{IV} = t_m$, substitution of (57) into (70) gives

$$R = \frac{0.2482}{\pi^2} \frac{b}{R} \left( \frac{f_m}{K_{dc}} \right)^2 \int_{-\theta_c}^{\theta_c} \int_0^R J(r, \theta) \frac{dr}{R}. \tag{71}$$

In light of the expression for the stress intensity factor given as $K_I = 1/\pi\sqrt{(2/b)} f(t)$ for the crack in Fig. 12, $f(t_{II})$ must satisfy the inequality $f(t_{II}) \geqslant \pi K_{dc}\sqrt{b/2}$. Introducing the dynamic coefficient $k$ into the inequality leads to

$$f(t_{II}) = \pi k K_{dc} \sqrt{\frac{b}{2}}. \tag{72}$$

Here $k$ is expected to contain the inertial effects on $K_{dc}$, including the velocity of crack propagation. From eqns (57) and (72), $f_m$ is given by

$$f_m = \frac{k\pi K_{dc}}{\sin\left( \frac{\pi}{2} \frac{t_{II}}{t_m} \right)} \sqrt{\frac{b}{2}}. \tag{73}$$

Substitution of eqn (73) into (71) leads to

Table 5. The dynamic coefficient $k$ varying with $b/R$ and $\theta_c$

| $b/R$ | $\theta_c$ (rad) | | | | | | | | |
|---|---|---|---|---|---|---|---|---|---|
| | 0.15 | 0.20 | 0.25 | 0.30 | 0.35 | 0.40 | 0.45 | 0.50 | 0.55 |
| 0.25 | 7.163 | 6.185 | 5.511 | 5.007 | 4.610 | 4.285 | 4.012 | 3.777 | 3.571 |
| 0.50 | 5.551 | 4.795 | 4.274 | 3.886 | 3.581 | 3.331 | 3.122 | 2.942 | 2.785 |
| 0.75 | 4.988 | 4.232 | 3.773 | 3.432 | 3.164 | 2.945 | 2.762 | 2.605 | 2.468 |
| 1.00 | 4.436 | 3.920 | 3.496 | 3.181 | 2.934 | 2.732 | 2.563 | 2.419 | 2.293 |
| 1.25 | 4.304 | 3.720 | 3.319 | 3.020 | 2.786 | 2.596 | 2.436 | 2.300 | 2.181 |
| 1.50 | 4.142 | 3.580 | 3.195 | 2.908 | 2.683 | 2.501 | 2.348 | 2.217 | 2.104 |
| 1.75 | 4.022 | 3.477 | 3.103 | 2.825 | 2.608 | 2.431 | 2.283 | 2.156 | 2.046 |
| 2.00 | 3.930 | 3.398 | 3.033 | 2.761 | 2.549 | 2.377 | 2.232 | 2.109 | 2.002 |
| 2.25 | 3.857 | 3.335 | 2.977 | 2.711 | 2.503 | 2.333 | 2.193 | 2.072 | 1.968 |

$$0.9676k^2\left(\frac{b}{R}\right)^2\int_0^{\theta_c}\mathrm{d}\theta\int_0^R J(r,\theta)\frac{\mathrm{d}r}{R}=1, \tag{74}$$

thus giving

$$k=1.017\left[\left(\frac{b}{R}\right)^2\int_0^{\theta_c}\mathrm{d}\theta\int_0^R J(r,\theta)\frac{\mathrm{d}r}{R}\right]^{-1/2}. \tag{75}$$

It follows that the dynamic coefficient $k$ is a function of $b/R$ and $\theta_c$. The numerical results listed in Table 5 for $\nu = 1/3$ show that $k$ is always greater than one. This is in agreement with its physical meaning and all known experimental results. Additionally, it is apparent from Table 5 that the formation of a large branching angle is more likely than the formation of a small one when $2\theta_c < 60°$.

*Acknowledgements*—The authors are gratefully indebted to Professor D. C. Leigh for his meticulous review of Section 2 of the manuscript and for his constructive suggestions towards the improvement of the paper. This project was financially supported by the Center for Robotics and Manufacturing Systems of the University of Kentucky. One of the authors (MTH) is grateful for support from N.S.F. under RIA grant No. MSS-9210531 during the course of this research.

## REFERENCES

Al-Hassani, S. T. S. and Johnson, W. (1969). The dynamics of the fragmentation process for spherical shells containing explosives. *Int. J. Mech. Sci.* **11**, 811–823.

Arakawa, K. and Takahashi, K. (1991a). Relationships between fracture parameters and fracture surface roughness of brittle polymers. *Int. J. Fract.* **48**, 103–114.

Arakawa, K. and Takahashi, K. (1991b). Branching of a fast crack in polymers. *Int. J. Fract.* **48**, 245–254.

Blackett, W. D. (1967). *Elementary Topology—A Combinatorial and Algebraic Approach*. Academic Press, New York.

Bowen, R. M. (1989). *Introduction to Continuum Mechanics for Engineers*. Plenum Press, New York.

Englman, R., Rivier, N. and Jaeger, Z. (1987). Fragment-size distribution in disintegration by maximum-entropy formalism. *Phil. Mag. B* **56**, 751–769.

Ewalds, H. L. and Wanhill, R. J. H. (1985). *Fracture mechanics*. Edward Arnold.

Ghosh, S. K. and Travis, F. W. (1979). An investigation into the static and dynamic piecing of diaphragms. *Int. J. Mech. Sci.* **21**, 1–22.

Grady, D. E. (1982). Local inertial effects in dynamic fragmentation. *J. Appl. Phys.* **53**(1), 322–325.

Grady, D. E. (1988). The spall strength of condensed matter. *J. Mech. Phys. Solids* **36**, 353–384.

Grady, D. E. (1990). Particle size statistics in dynamic fragmentation. *J. Appl. Phys.* **68**(12), 6099–6105.

Grady, D. E. and Kipp, M. E. (1985). Geometric statistics and dynamic fragmentation. *J. Appl. Phys.* **58**(3), 1210–1222.

Griffith, A. A. (1920). The phenomena of rupture and flow in solids. *Phil. Trans. R. Soc. London* **A221**, 163–197.

Gulden, M. E. (1979). *Solid Particle Erosion of High Technology Ceramics*. ASTM, STP664, Philadelphia.

Irwin, R. G. (1957). See Tada, H., Paris, P. C. and Irwin, G. R. (1973). *The Stress Analysis of Cracks Handbook*. Del Research Corporation, Hellertown, PA.

Isida, M. and Noguchi, H. L. (1992). Stress intensity factors at tips of branched cracks under various loadings. *Int. J. Fract.* **54**, 293–316.

Johnson, W. (1972). *Impact Strength of Materials*. Edward Arnold, London.

Kanninen, F. M. and Popelar, C. H. (1985). *Advanced Fracture Mechanics*. Oxford University Press, New York.

Kimball, W. S. (1952). *Calculus of Variations*. Butterworths, London.

Kipp, M. E. and Grady, D. E. (1985). Dynamic fracture growth and interaction in one dimension. *J. Mech. Phys. Solids* **33,** 399–415.

Kobayashi, A. S., Seo, K., Jou, J. Y. and Urabe, Y. (1980). A dynamic analysis of modified compact-tension specimens using homalite-100 and polycarbonate plates. *Exp. Mech.* **20,** 73–79.

Kobelev, V. V. (1990). Fragmentation of a composite material and fragmentation of fibers under a dynamic load. *PMM* **54,** 577–581.

Lankford, J. and Blanchard, C. R. (1991). Fragmentation of brittle materials at high rates of loading. *J. Mater. Sci.* **26,** 3067–3072.

Leigh, D. C. (1968). *Nonlinear Continuum Mechanics.* McGraw-Hill, New York.

McKnight, D. S. (1991). Determination of breakup initial conditions. *J. Spacecraft Rockets* **28,** 470–476.

Meakin, P. (1991). Models for material failure and deformation. *Science* **252,** 226–234.

Meyerhoff, R. (1992). Geometric invariants for 3-manifolds. *Math. Intelligencer* **14,** 37–53.

Mott, N. F. (1948). Fracture of metals: Some theoretical considerations. *Engineering* **165,** 16–18.

Ramulu, M. and Kobayashi, A. S. (1985). Mechanics of crack curving and branching—a dynamic fracture analysis. *Int. J. Fract.* **27,** 187–201.

Ramulu, M., Kobayashi, A. S. and Kang, B. S. J. (1984a). Dynamic crack branching—a photoelastic evaluation. *Fract. Mech.* ASTM STP 883, 130–142.

Ramulu, M., Kobayashi, A. S., Kang, B. S. J. and Barker, D. B. (1984b). Further studies on dynamic crack branching. *Exp. Mech.* **23,** 431–437.

Schardin, H. (1959). Velocity effects in fracture. *Fracture,* 297–330.

Slate, P. M., Billings, M. J. and Fuller, P. J. (1967). The rupture behavior of metals at high strain rates. *J. Inst. Metals* **95,** 244.